Analysis of conduction mechanism in lamellar double hydroxide by impedance spectroscopy

ABDERRAHMANE   ELMELOUKY[a], RADDAD   EL MOZNINE[a], REDOUANE   LAHKALE[b], RACHID   SADIK[b], ELMOULOUDI   SABBAR[b], EL GHAOUTI   CHAHID[a], ELHASSAN   CHOUKRI[c], DAOUD   MEZZANE[c], AIMAD BELBOUKHARI[c]

[a]*Laboratoire de Physique de La Matière Condensées (LPMC). Université Chouaib   Doukkali, Faculté des sciences, El-Jadida, Morocco*
[b]*Laboratoire de Physicochimie des matériaux(LPCM). Université Chouaib Doukkali, Faculté des sciences, El-Jadida, Morocco*
[c]*Laboratory of the Condensed Matter and Nanostructures LMCN Faculty of Science and Technique FST – Gueliz*

Zn-Al layered double hydroxides (LDHs) were prepared; using the co-precipitation method; with Cl⁻ and NO3⁻interlayer anions and with two Zn / Al ratio (R=2 and R=3). The structural evolution of these compositions was characterized by Riveted analysis on powder X-ray diffraction diagrams. Impedance measurements of these compositions were investigated in the frequency range [100Hz–1MHz] and in the temperature range 25 °C - 90°C. Cole–Cole plots in impedance spectra showed non-Debye relaxation. The temperature dependence of the relaxation times for all samples showed Arrhenius behavior, from which the activation energy was derived. The real part of ac conductivity spectra of these materials obeys Jonscher power law. The nature of variation of the electrical conductivity, and value of activation energy of different samples, suggest that the conduction process appear clearly related to the structural evolution of the interlayer domain.

1. Introduction

Layered double hydroxides (LDHs), also called anionic (anion-exchanging) clays and hydrotalcite-like compounds [Allmann 1970][1] are layered compounds that are based in brucite, Mg (OH). They have a stacking of positively charged octahedral sheets with:

$$\left[M_{1-x}^{II} M_x^{III} (HO)_2 \right]^{x+}$$
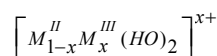
The compositions M^{II} and M^{III} are divalent and trivalent metal ions (Zn, Al), respectively. The net positive charge, due to substitution of trivalent by divalent metal ions, is balanced by an equal negative charge of Interlayer solvated anions: $\left[X_{x/m}^{m-} \, nH_2O \right]^{x-}$

The hydrated anions in the interlayer spaces can be replaced with almost any desired anion, organic or inorganic, by utilizing simple ion exchange methods.

These compounds showed clearly the M (OH) $_2$ brucite-like main layers, the anionic interlayer domains containing chloride ions and water molecules.

In previous works [2–4], the conductivity of LDHs based on different M^{II}-M^{III} pairs, various interlamellar anions and hydration amounts nH_2O were studied; the mainly protonic conduction process was demonstrated by impediantiometric (HP) measurements in an electrochemical gas cell. However, no study has been performed in relation to the structural evolution of these

compounds. This particular system was selected to the wide range of different trivalent metal amounts that can be obtained.

Impedance spectroscopy [4] was used to investigate evolution of ionic conductivity; in a family of Lamellar Double Hydroxides (LDH) with a general formula:
$[Zn_{1-x} Al_x(OH)_2]^{x+}[Cl_x.nH2O]^{x-}$ In a short notation:
$(Zn_{1-x}Al_x (OH)_2X_x.nH_2O)$
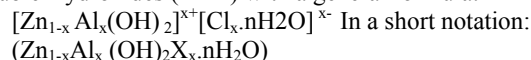
These compounds are usually abbreviated as [M^{II}-M^{III}-X] they are characterized by high charge density of sheets, modulated via the M^{II}/M^{III} ratio.

Zn_RAl/Cl^- and Zn_RAl/CO_3^{2-} phases [5] were obtained with a broad range of divalent and trivalent metal contents, defined by $x=M^{II} / M^{III} + M^{II}$ with $x_{feuillet}$=0.25 and 0, 33. In this range of composition, they display a clear evolution of lattice and structural parameters, but the rhombohedral stacking sequence of the layers is preserved. The positive charge density of these layers is directly proportional to x.

The aim of the present work was to prepare Zn-Al LDHs of different Zn/Al ratios (R= 2 and 3) with Cl⁻ or NO3⁻ in the interlayer space. The exchange ability of interlayer anions depends both on their formal charge (monovalent anions) and on their intrinsic nature (Nitrogen N is strongly held).

These compositions have been characterized using X-ray diffraction XRD and ICP techniques. Impedance measurements were also used to analysis of the conduction mechanism in theses compositions. As a first steps; a comparison of the obtained results for Cl anion with those obtained by Ducos et al on only the Cl anion [4].

Secondly; the effect of the substituent of Cl^- by NO_3^- is disssed:

2. Experimental details

2.1 Preparations of samples

The Zn_RAlX $(X = Cl^-, NO_3^-)$ phases are prepared by the co-precipitation method [5] under CO_3^{2-} free conditions in a 1l vessel, by slow addition of molar solutions of metallic salts in appropriate proportions. The precipitation was performed at constant pH (pH=8) by a controlled addition of a molar sodium hydroxide solution, leading to quantitative precipitation of the metallic salts. The obtained microcrystalline phases were then carefully washed by three cycles of centrifugation/dispersion in de-ionized water, in order to remove the adsorbed electrolytes sodium Chloride four matrixes Zn_RAlX: $(X = Cl^-, NO_3^-)$.

Phases were obtained with the following trivalent metal amounts: $x_{feuillet}$= 0.25 and 0.33.For higher or lower values of $x_{feuillet}$, secondary phases are observed; the study of the corresponding mixed phases is not reported here. All precursors Zn_2AlNO_3, Zn_3AlNO_3, Zn_2AlCl, Zn_3AlCl were synthesized by coprecipitation method as described [1]. In a reaction medium consisting of distilled water initially, aqueous solutions of metallic salts are added at a constant rate and under nitrogen to prevent contamination by CO_3^{2-} . The pH being kept constant at a value of 8 by the controlled addition of a basic solution consisting of NaOH. After 24 hours of curing, the mixture was centrifuged and washed several times with 5 decarbonated water and finally dried 50 ° C overnight and then ground for analysis.

2.2 X-ray diffraction

The X-ray diffraction patterns were carried out on **D2-PHASER** of **BRUKER-AXS diffractometer** which used K α_1 (1.54056 Å) and K α_2 (1.54439 Å). Generator used at 30 kV and 10 mA. Computation time 15 and 70° (2θ) by step of 0.0101° (0. 2 s by step). Program duration is 18mn 06 s.

2.3 Induced coupled plasma (ICP) measurements

The metallic ratio what were performed using ICP measurements. A plasma or gas consisting of ions, electrons and neutral particles, is formed from Argon gas, which is then utilized to atomize and ionize the elements in the sample matrix. These resulting ions are then passed through a series of apertures into a high vacuum mass analyzer where the isotopes of the elements are identified by their mass-to-charge ratio The intensity of a specific peak in the mass spectrum is proportional to the amount of the elemental isotope from the original sample, this technique of choice in many analytical for providing the accurate and precise measurements.

Table.1. Elemental Chemical Analysis Data (Metals ratio, (%) weight of Al and Zn at different anions

Samples	(%) Zn	(%) Al	R_{exp}	R_{th}
Zn_2AlCl	36.9	7.8	1.95	2
Zn_3AlCl	45.4	6.4	2.93	3
Zn_2AlNO_3	34.5	7.3	1.95	2
Zn_3AlNO_3	42.8	6.0	2.93	3

3. Impedance measurements

The impedance measurements were carried out with a 4192 A LF Impedance Analyzer (Hewlett Packard) between 100 Hz and 1 MHz a source of 1V was applied to the electroded pellet samples. The temperature variation was performed using a hot stage with a temperature stability of ± 0.1 K. Silver electrodes were deposited on two circular faces of the sample to get the capacitor shaped samples.

The diameter and the thickness of the sample were 13 mm and 1 mm, respectively. Curve fitting of dielectric spectra with complex empirical functions was carried out using commercial Zview software (version 2.2).

4. Results and discussion

4.1 Structural study

Previous structural results [6–8] were used as a starting point. The rhombohedral symmetry (R3m space group) is described in its hexagonal setting. The a lattice parameter corresponds to the mean distance between two metallic cations in the brucitic layers, and the c lattice parameter to three times the basal spacing of these layers.

The structural parameters were obtained by the Rietveld method [9] with the Fullprof program [10].Both metallic cations are statistically distributed in 3a positions of the space group, hydroxyl groups are in (6c), and the interlayer species chloride and oxygen atoms of water molecules are also statistically distributed on the high multiplicity 18(g) position with low (1/6) occupancy.

Fig. 1 shows the X-ray diffraction pattern of the all composition. From the analysis of the spectra, the materials crystallize in the $R3m$ space group

(Rhombohedral phase) with: $c/3 = d_{003} = 2 \times d_{006}$ and a (intermetallic distance) $= 2 \times d_{110}$.

The cell parameters of the four samples are included in table 2. The c parameter (which represents the thickness of three layers plus the interlayer space between them) was calculated from the average of (00l) reflections. The c parameter decreases as the M^{II}/M^{III} ratio decreases, what has been assigned [11] to stronger interactions between the layers and the interlayer anions.

The structural study gives, notably, access to the evolution with x of the lattice parameters and interatomic distances. The evolution of the lattice parameter a is quite linear with x according to equation [12]:

$$a = \sqrt{2} \cdot \left(\left(1 - x_{feuillet}\right) \cdot r_{M^{II}} + x_{feuillet} \cdot r_{M^{III}} \right)$$

And is attributed to the corresponding evolution of the mean ionic radius of metallic cations, respectively, 0.74 and 0.53 Å for Zn^{2+} and Al^{3+} the c lattice parameter, which is directly related to the interlayer distance display, also decreases values when x increases. This behavior was previously reported [11] and attributed to the increase of charge density on the brucitic layers, leading to stronger interactions with the interlayer anions, although the interlayer domains become more encumbered by the larger chloride anions. We observe in [12] a clear non-linear evolution of c, with a faster decrease at the lowest values of $x_{feuillet}$ [13].
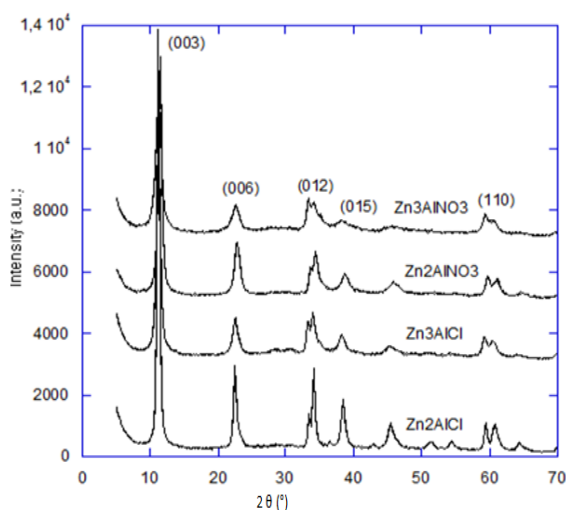
Fig.1.X-ray diffractograms

Table.2.values of the lattice parameters c, a and percentage of water for all compositions.

Samples	c(Å)	a(Å)	(°/°) of H_2O
Zn_2AlCl; R=2	23.7179	3.1032	16
Zn_3AlCl; R=3	23.8278	3.1072	8
Zn_2AlNO_3,R=2	23.2035	3.0894	14.2
Zn_3AlNO_3;R=3	23.6226	3.1026	7.4

4.2 Induced coupled plasma (ICP)

The chemical compositions of the different LDH are included in Table 1, which shows that the $[Zn^{2+}/Al^{3+}]$ ratio in the solids is close to that in the starting solutions. The formula in the table considers that chloride is the only compensating anion and does not take into account the possible presence of carbonate impurities in the interlayer space, even for NO_3^-.

This characterization also suggests that the samples have a homogeneous chemical composition, the approximate Chemical formula is:

$(Zn_{2.93}Al (OH)_{7.86})(NO_3^-, 1.84\ H_2O)$ for ratio R=3, $X=NO_3^-$
$(Zn_{2.93}Al (OH)_{7.86})(Cl^-, 1.87\ H_2O)$ for ratio R=3, X= Cl^-
$(Zn_{1.95}\ Al (OH)_{5.9})(NO_3^-, 2.93\ H_2O)$ for ratio R=2, $X=NO_3^-$
$(Zn_{1.95}Al (OH)_{5.9})(Cl^-, 3.07\ H_2O)$ for ratio R=2, X= Cl^-

4.3 Impedance spectroscopy measurement
4.3.1 Complex impedance spectra

Fig. 2(a); (b) and Fig. 3(a); (b) shows the evolution of the imaginary part Z" as a function of the real Z' in the frequency range $100Hz–10^6Hz$ and at different temperature for all compositions. All samples compositions show the q similar behavior. At lower temperatures Z" linearly increases with Z'. When temperature increases the semi-circles become smaller, providing the shift towards lower |Z|. This indicated a reduction of the resistance of the sample. The semi-circles are not perfect but skewed (inclined) with their centers depressed below the real Z'-axis by an angle $(\alpha-1) \times \pi/2$, where $0<\alpha<1$ [14], that indicates the presence of non-Debye type relaxation phenomena caused by a distribution of relaxation time.

The complex impedance plane plots (Z" vs. Z') are commonly used to separate the bulk material and the electrode surface polarization phenomena [15, 16, 17–19, 20, 21, 22]. A common feature of samples with dc conductivity is a discontinuity at electrode/sample interface, which has different polarization properties with the bulk material.

In the complex impedance plane plot (Z" vs. Z') of the MMT clay colloidal suspension in PVP-EG blend [23]; all plots have two separate arcs, which are corresponding to the bulk material effect (the upper frequency arc) and the electrode surface polarization (the lower frequency arc) [15, 16, 17–19, 22, 23]. The frequency values correspond to Z" minimum value in the plots separates the bulk material and electrode polarization phenomena.

In complex impedance plots; the diameter of arc gives the value of bulk resistance R_{dc} of the sample and hence the σ_{dc} values [15]. It is observed that the R_{dc} of these sample decreases with the increase of temperature; and hence the σdc values increases.

The existence of depressed semi-circles in impedance spectra can be explained by a number of phenomena, depending on the nature of the investigated system. In general, the impedance data can be represented as an equivalent circuit, which consists of two parallel of resistance (R) and constant phase element (CPE) in series. This is the one of the most common interpretation of phenomena for polycrystalline having a contribution of bulk grain, grain boundary and electrodes [16]. In our measurements; the lowest frequency value (100 Hz) imposed by the instrument HP; the only one arc observed can be attributed to the only bulk contribution of the

sample. Therefore; the equivalent electrical circuit was reduced the only one parallel resistance (R) and constant phase element (CPE) to represent the only bulk contribution.
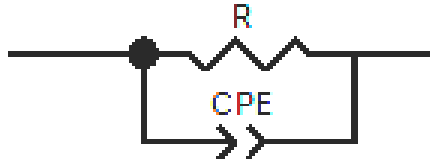
Equivalent electrical circuit
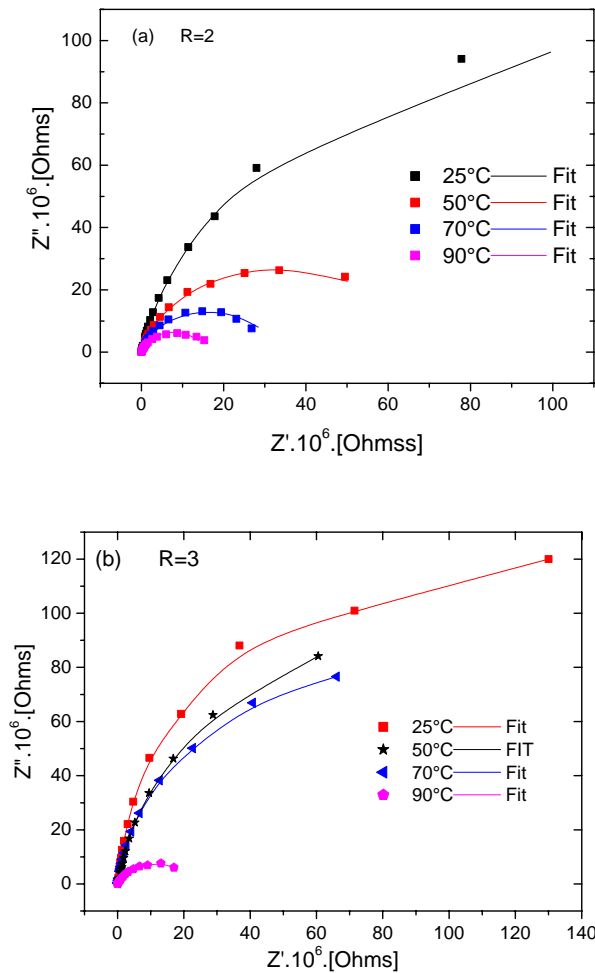
Fig. 2. (a); (b) . Complex plane plots (Z'' v.s Z') of Zn_RAlCl for R=2 (a) and R=3(b).
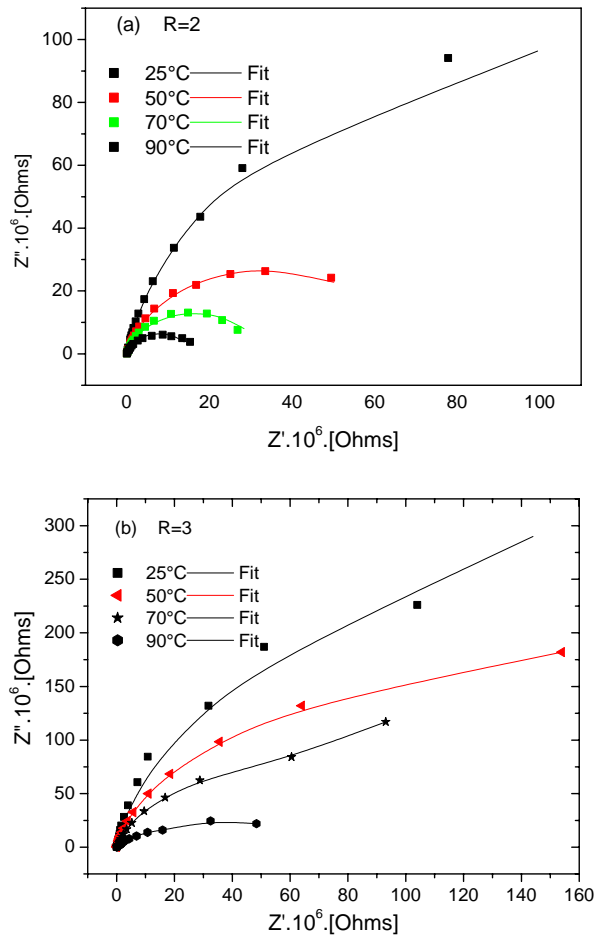
Fig. 3. (a, b) Complex plane plots (Z'' v.s Z') of $Zn_RAlNO_3^-$ for R=2 (a) and R=3(b).

The impedance of constant phase element (CPE) can be described as [24]:

$$Z^*_{CPE}(\omega) = \frac{1}{T(j\omega)^p} \qquad (1)$$

where ω is the angular frequency, T and p are constants and $0 < p < 1$. The CPE describes an ideal capacitors with C=T for p=1 and an ideal resistor with R=1/T for p=0. The, p can be used to represent the degree of perfection of the capacitor and represents a measure of arc distortion below the real impedance axis. The parameter p is related with the depression angle as follow:

$$\alpha_d = (1-p) \times \frac{\pi}{2}$$

The complex impedance (Z*) of such circuit (CPE//R) is as follow:

$$Z^*(\omega) = \frac{R}{1 + RT(j\omega)^p} \qquad (2)$$

The equation (2) can be written as.

Where: $\tau^p = RT$

$$Z^*(\omega) = \frac{R}{1 + (j\omega\tau)^p} \qquad (3)$$

$$\omega_{max} = \tau^{-1} = (RT)^{-1/p}$$

It is important to see that the shape of the equation (3) in impedance complex $Z^*(\omega)$ is similar to the Cole-Cole relaxation in the complex permittyivity $\varepsilon^*(\omega)$; except the R at high frequency . Such relaxation is commonly used to analysis the behavior of ionics conductors [25-26].

In ower case; this later value is close to 0. Therefore The serie resitance was not added in the circuit.

The maximum in the imaginary part $Z'(\omega)$ occurs at

$$\omega_{max} = \tau^{-1} = (RT)^{-1/p}$$

The curve fit of the experimental data was obtained in the whole frequency range using the constant phase element (CPE) as shown in Figure 2(a); (b) and Fig. 3 (a); (b).

The resistance R, and the parameters p and T of the CPE were obtained for each temperature. The values of p are found to lie close to unity (between 0.72 and 0.98). The constant time (τ) of relaxation were then obtained using the relationship given in equation (3). The dc conductivity was derived from the resistance. Table .3 give the value of the dc conductivity (σ_{dc} a) and the relaxation time (τ) of alls compositions.

Table 3: Parameters obtained from fitting circuit

Anion Cl⁻	σ_{dc} (S/m) 10^3	τ (ms)
R=2	4.33	0.63
R =3	1.93	0.97
Anion NO₃⁻	σ_{dc} (S/m)	τ (ms)
R=2	2.10	1.36
R=3	1.14	1.16

4.3.4 Ac Conductivity spectra

Figs. 4. (a), (b) and 5 (a), (b) show the frequency dependence of σ_{ac} conductivity at several temperatures for both clay samples (Cl⁻) and (NO₃⁻) respectively. It shows a plateau at low frequencies and dispersion at high frequencies. The plateau region corresponding to dc conductivity is found to extend to higher frequencies when temperature increases. The frequency at which the

dispersion takes place, also known as hopping frequency, increases with increasing of the temperature T. This behavior suggests that electrical conductivity occurs via hopping mechanism, which is governed by the Jonscher's power law [24-25].

$$\sigma_{ac}(\omega) = \sigma_{dc} + A\omega^n \qquad (4)$$

Where, σ_{dc} is the direct current conductivity of the sample, ω the angular frequency of measurement. The exponent represents the degree of interaction between mobile ions and with the lattices around them and A is a constant which determines the strength of polarizability.

The frequency dispersion has been attributed to ac conductivity whereas the frequency-independent behavior of conductivity in the plateau region corresponds to dc conductivity.

Since the complex conductivity $\sigma^*_{ac}(\omega)$ is related to the complex admittance. This latter can be deduced from the equation (3):

$$Y^*(\omega) = \frac{1}{R} \cdot \left[1 + (j\omega\tau)^p\right]$$

$$Y^*(\omega) = Y'(\omega) + j\, Y''(\omega) \qquad (4)$$

The real and imaginary parts can be written as follow:

$$Y'(\omega) = \frac{1}{R}\left[1 + (\omega\tau)^p \cos\left(\frac{p\pi}{2}\right)\right] \qquad (5)$$

$$Y''(\omega) = \frac{1}{R}\left[1 + (\omega\tau)^p \sin\frac{p\pi}{2}\right] \qquad (6)$$

The real part Y' of function the admittance is related to the ac conductivity $\sigma_{ac}(\omega)$.

$$\sigma_{ac}(\omega) = \frac{e}{S} \times Y'(\omega)$$

Where k is the cell constant: $\qquad k = \frac{e}{S}$

$$\sigma_{ac}(\omega) = \left[\frac{e}{S} \times \frac{1}{R}\right] + \left[\frac{e}{S} \times \frac{1}{R} \times \tau^p \cos\left(\frac{p\pi}{2}\right)\right] \times \omega^p \qquad (7)$$

The direct current conductivity σ_{dc} can be calculated by the following expression:

$$\sigma_{dc} = \frac{e}{S} \times \frac{1}{R} = k \times \frac{1}{R}$$

In the equation (7) the constant A is attributed to the following expression:

$$A = \sigma_{dc} \times \left[\tau^p \cos \frac{p\pi}{2} \right]$$

$$\sigma_{ac}(\omega) = \sigma_{dc} + A\omega^p$$

Therefore the equation (7) becomes the well known Jonscher's power law given in equation (4).

The solid line in the σ' spectra represent the fit of experimental data to the Jonscher's power law. The fit values of σ_{dc}, A and n were obtained by Origin non-linear curve fitting software. The values of σ_{dc}, are very close to those obtained from R values in the equivalent circuit.
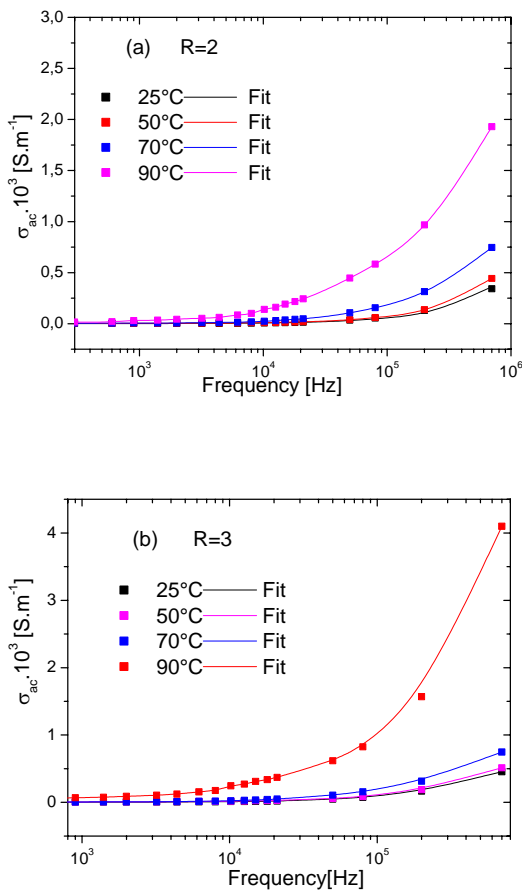
Fig. 4(a), (b). Frequency dependence real part of ac conductivity of Zn₂AlCl (R=2) and Zn₃Al Cl (R=3).
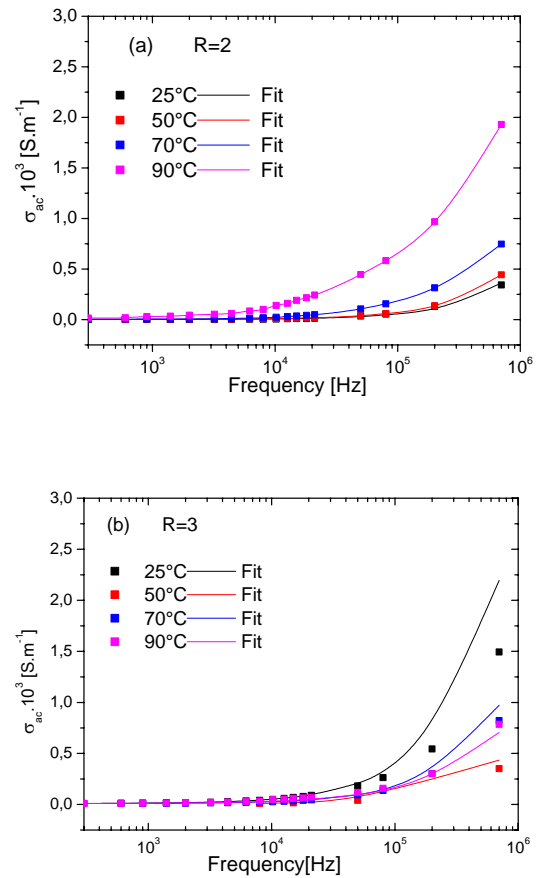
Fig. 5 (a), (b). Frequency dependence real part of ac conductivity σ_{dc} of Zn₂AlNO₃ (R=2) and Zn₃Al NO₃ (R=3)

The evaluated σ_{dc} are also plotted against 1000/T in Fig. 6 for alls compositions. The linear regression suggests Arrhenius behavior.

$$\sigma_{ac}(T) = \sigma_{dc} \exp(-E/k_BT) \qquad (9)$$

The activation energy values were calculated using the Arrhenius equation (9) for the four compositions and are given in Table 5. The activation energies obtained in the experiment are typical value for an ionic conductor temperature presented in the representation of effect of interlayer anion as it is reported by Dugos and all [4].

*Table 4. Values of the activation energy and the
correlation factor R from the linear fit.*

Samples	E_a (eV)	R
Zn_2AlCl	0.64	0.99
Zn_3AlCl	0.50	0.97
Zn_2AlNO_3	0.49	0.98
Zn_3AlNO_3	0. 41	0.99
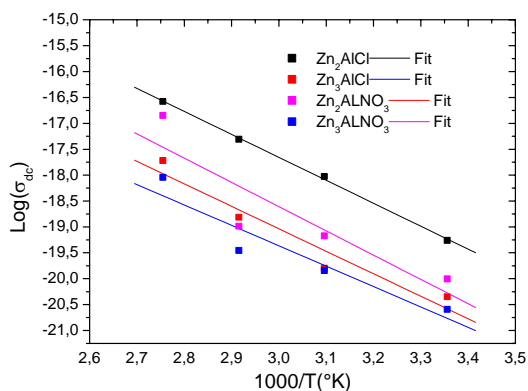
*Fig. 6.Evolution of σ_{dc} as a function the temperature for
all compositions.*

Effect of the ratio R on the structural parameters

The structural study gives access to the lattices
parameters a and c as it is reported in Table.2. The a lattice
parameter corresponds to the mean distance between two
metallic cations in the brucitic layers, and the c lattice
parameter to three times the basal spacing of these layers.
The analysis of the structural parameters a obtained by
XRD show that:

For Cl⁻ anion.
the values of a lattice parameter ; are respectively
3.1032 A° and 3.1072 Å for R=2 (x = 0.33) and for R=3
(x = 0.25) . The increase of x or the decrease of R lead to
the decreases of the a lattice parameter. This behaviour
was also found by Ducos et al [4]. It is attributed to the
corresponding size of the mean ionic radius of metallic
cations; which are 0.74 and 0.53 Å respectively.
Concerning the values of c lattice parameter; which is
directly related to interlayer distance; the values of c
lattice parameter; are respectively 23.7179 Å and 23.8278
Å for R=2 (x = 0.33) and for R=3 (x = 0.25) . That
means the c lattice parameter decreases when the x
increases. The same behavior was previously also
reported by Ducos et al [4] and it was attributed to the
increase charge density on the brucitic layers; leading to
strong interactions with the inert-layer domains become
more encumbered by the larger chloride anions. A non-
linear evolution of c; with a decreases faster at the lowest
values of the x than at the highest; corresponding to the
opposite contribution of electrostatic interactions; and
basically; Vander Waals interactions between protons of

the hydroxyl group and protons of the interlayer water
molecules. It is important to state that the non linear
started from x = 0.35. Thus these results are in good
argument with those obtained by Ducos et al [4].

For NO_3^- anion.
The values of a lattice parameter; are respectively
3,0894 A° and 3.1026 Å for R=2 (x = 0.33) and for
R=3 (x = 0.25). The values of c lattice parameter; are
respectively 23.2035 Å and 23.6226 Å for R=2 (x = 0.33)
and for R=3 (x = 0.25). That means the a and c lattices
parameter decreases when x increases. The same behavior
as in the case of Cl⁻ anion. In this case; it seems important
to compare the amount of water H_2O:
The amount of H_2O; are respectively 16 % and 8 %
for R=2 (x = 0.33) and for R=3 (x = 0.25). The increase of
x leads the increase of % of the water because the
interlayer species (chloride and oxygen atoms of water
molecules) are distributed on the high multiplicity (18g)
position with low 1⁄6 occupancy [4]. As for NO_3^- anion⁻;
the amount of H_2O; are respectively 14 and 7.4 for R=2 (x
= 0.33) and for R=3 (x = 0.25). This means that the
increase of x lead the increase of % of the water. This can
be attributed to the increase of the interlayer species NO_3^-
anion as is the case of Cl⁻ anion. However; the amount of
the water evaluated in the case of NO_3^- is less than of Cl⁻
anion.

Effect of the substitution of Cl⁻ anion by NO_3^-.

The values of c lattice parameter obtained by XRD;
which is directly related to interlayer distance as it is
discussed previously; show that:
For R=2 (x = 0.33); the values of c lattice parameter;
are respectively 23.7179 Å and 23.2035 Å for Zn_2AlCl
and Zn_2AlNO_3. For R=3 (x = 0.25); the values of c lattice
parameter ; which is directly related to interlayer distance;
are respectively 23.8278 Å and 23.6226 Å for Zn_2AlCl
and Zn_2AlNO_3. This suggests that the network (Cl⁻/ H_2O)
is much less compact since the inter-lamellar distance is
higher. In contrast, the network (NO_3^-/H_2O) have a
hydrogen bond network grow on the surface of the sheets,
resulting in a network more compact.
In Table 6 and 7; we reported the value of the
conductivity; activation energies; the relaxation time
obtained from impedance measurements the amount of the
water in each composition with the different type of anions
for R= 2 and R=3 respectively.

*Table 6: values of the conductivity; activation energy;
the relaxation time and of the %water For R=2*

Anions	Cl⁻	NO_3^-
$\sigma_{dc} 10^3 (S.m^{-1})$	4.33	2.10
E_a (eV)	0.64	0.49
τ (ms)	0.63	1.36
(%) of H_2O	16	14

*Table .7. Values of the conductivity; activation energy;
the relaxation time and of the %water For R=3*

Anions	Cl^-	NO_3^-
$\sigma_{dc\ (10^{-3}}$	1.93	1.14
E_a (eV)	0.50	0. 41
τ (ms)	0.97	1.16
(%) of H_2O	8	7.4

For both case (R=2 and R=3); the substation of Cl^- anion by NO_3^- lead to the decrease of the conductivity and the activation energy. In contrast; the constant time relaxation increases. It follows that the fast relaxation times and large activation energies correlate with the greater percentage of the water. In addition this behavior correlate well with the comparison of the values of c lattice parameter obtained by XRD; which is directly related to interlayer distance. Indeed; the substation of Cl^- anion by NO_3^- lead to the decrease of the c lattice parameter. This later decrease gives a less compact for Cl^- anion since the inter-lamellar distance. In contrast, for NO_3^- anion would have a more compact since the inter-lamellar distance is lower. This behaviour can explain the low constant relaxation time (τ) as a fast process) for Cl^- anion compared to NO_3^- anion; which show the high constant relaxation time (τ) as a slower process).

The observation that the activation energy decreases with the substitution of Cl^- anion by NO_3^- suggests that negative sites act to trap the protons that would otherwise remain mobile in the matrix. It is probable that charge transport occurs via the hopping of protons between ionizable sites. In the system under investigation, the origins of these charge sites are partly due to self dissociation of the O–H groups from the matrix and water [24].

The differences in relaxation times and activation energies when the Cl^- anions is substituted by NO_3^- must therefore be explained in terms of the differences in the way in which this water interacts with the kind of anions in the matrix .

The observation that the activation energy decreases with the substitution of Cl^- anion by NO_3^- suggests that negative sites in the case NO_3^- anions act to trap the protons that would otherwise remain mobile in the matrix.

The mean diffusion path length is a function the availability of diffusible protons and of the negative sites.). There is a greater probability that a proton will be trapped by the negative site of oxygen. Therefore, the presence of the more negative sites of oxygen reduces the mean diffusion path length and explains the shorter relaxation times observed for the NO_3^- anions.

5. Conclusion

The XRD analysis showed that these compositions of layered double hydroxides (LDHs); which were prepared with Cl^- and NO_3^- interlayer anions and with two ratio (R=2 and R=3) of Zn∕Al; are well crystallized.

The structural study allowed to evaluate to the a and c lattice parameters. The obtained values of c lattice parameter; which is directly related to interlayer distance indicated that the substitution of Cl^- anion by NO_3^- lead to the decrease of the c lattice parameter resulting in a less compact for Cl^- of the inter-lamellar distance. Whereas, for NO_3^- anion a more compact since the inter-lamellar distance is lower.

Impedance spectroscopy was also used to investigate the conduction mechanism in these compositions. The temperature dependence of the σ_{dc} conductivity for all samples showed Arrhenius behavior, from which the activation energy was derived. Arrhenius behavior; which is consistent with thermally activated proton transport; as the underling mechanism of the conduction process. A protonic charge transfer process is suggested as the principle cause of the conduction behavior.

So far we can not examine the evolution of the structural parameters with x since only tow compositions were prepared. Other compositions are under investigation in order to analysis the evolution of the structural parameters with x in the both cases of anions.

Since to the imposed experimental limit at low frequency is 100 Hz, it was not clear to examine the low frequency behavior such a electrode polarization and the low frequency dispersion. Therefore; the next impedance measurements will be carried out at least up down to 10^{-1} Hz. This could be a help full to establish a possible correlation between the fit parameters and the conduction mechanism in such complex system; when the Cl^- anion is substituted by NO_3^-.

References

[1] Shigeo Miyata, Clays and Clay Minerals, **23**, 369 (1975). Pergamon Press. Printed in Great Britain

[2] A. de Roy, C. Forano, E.M. Khaldi, J.P. Besse, Anionic clays: trends in pillaring chemistry, inOcelli Robson Eds., Synthesis of Micro porous Materials vol. 2, Van Nostrand Reinhold, New York, 1992, pp. 108 169.

[3] Y. Li, R. Zhang, H. Chen, J. Zhang, R. Suzuki, T. Ohdaira, M. M. Feldstein, Y. C. Jean, Biomacromolecules, **4**, 1856 (2003).

[4] V. Ducos, A. de Roy), J.P. Besse, Solid State Ionics **145**, 399 (2011).

[5] S. Miyata, Clays Clays Miner. **23**, 369 (1 975)

[6] V.R. Allmann, Chimia **24**, 99 (1970).

[7] S. Kim, E-J. Hwang, Y. Jung, M. Han, S-J. Park, Colloids and Surfaces A, **313– 314**, 216 (2008).

[8] D. K. Pradhan, R. N. P. Choudhary, B. K Samantaray, Express Polymer Letters, **2**, 630 (2008).

[9] M.H. Rietveld, J. Appl. Crystallogr. **2** 65 (1969).

[10] J. Rodrigues-Carvajal, Fullprof Program III, Grenoble, France, 1994.

[11] M.J. Avena, Acid–base behavior of clay surfaces in aqueous media. In: Hubbard, A. (Ed.), Encyclopedia of surface and colloid science. Marcel Dekker, New York, 2002pp. 17–46.

[12] Brian Gregoire, thèse Relation Composition-Structure des Hydroxydes Doubles Lamellaires: Effets de la charge du feuillet et de la nature de l'anion interfolaire.

[13] M. Oleinikova, M. Munoz, J. Benavente, M. Valiente, Anal. Chimi. Acta **403,** 91 (2000).

[14] R. J. Sengwa, S. Sankhla: Polymer Bulletin, **60**, 689 (2008)

[15] S. Kim, E-J. Hwang, Y. Jung, M. Han, S-J. Park, Colloids and Surfaces A**, 313–314**, 216 (2008).

[16] D. K. Pradhan, R. N. P. Choudhary, B. K. Samantaray, Express Polymer Letters, **2**, 630 (2008).

[17] R. J. Sengwa, S. Sankhla, Colloid and Polymer Science, **285**, 1237 (2007).).

[18] R. J. Sengwa, S. Sankhla, Journal of Macromolecular Science Part B: Physics, **46**, 717 (2007).

[19] R. J. Sengwa, S. Sankhla, Indian Journal of Engineering and Materials Sciences, **14**, 317 (2007).

[20] P. Pissis, A. Kyritsis, Solid State Ionics, **97**, 105 (1997).

[21] R. J. Sengwa, S. Sankhla, Polymer **48**, 2737 (2007).

[22] A. K. Thakur, D. K. Pradhan, B. K. Samantaray, R. N. P. Choudhary, Journal of Power Sources **159**, 272 (2006).

[23] R.J. Sengwa, S. Choudhary, S. Sankhla, Express Polymer, Letters **2**(11), 800 (2008).

[24] R. El Moznine, G. Smith, E. Polygalov, P.M. Suherman, J. Brodhead, J. Phys. D, **36**, 330 (2003).

[25] Y. Amira, thesis, University Cadi Ayyad 2010, p. 85

[26] F. De Guerville, M. El Marssi, I. Luk'yanchuk, L. Lahoche, Ferroelectrics **359**, 14 (2007), State Ionics **8**, 159 (1983).

[27] P.B. Macdo, C.T. Moynihan, R. Bose, Phys. Chem. Glasses **13**, 171 (1972).

[28] N. Hirose, A.R. West, J. Am. Ceram. Soc. 79 (1996) 1633.

[29] R.C. Buchanan, Ceramic Materials for Electronics 1992.

---

[*]Corresponding authors: elmoznine@yahoo.fr
elmlouky_abderrahmane@yahoo.fr;